# First-principles calculations of cohesive energies in the Al-Co binary alloy system

M. Mihalkovič* and M. Widom
*Department of Physics, Carnegie Mellon University, Pittsburgh, Pennsylvania 15213, USA*
(Received 3 August 2006; published 10 January 2007)

The phase diagram of the Al-Co binary alloy system is intensively studied because of its importance for understanding decagonal quasicrystals, but remains imprecisely known due to the occurrence of many competing complex structures with composition close to $Al_{13}Co_4$. We apply first-principles total energy calculations to compare the cohesive energies of known and hypothetical structures. Our results confirm the experimentally established phase diagram in every detail except near $Al_{13}Co_4$, where the reported phases (Pearson symbols mC102 and oP102, both well-known decagonal quasicrystal approximants) turn out to be unstable at low temperatures. They may be stabilized at high temperatures by the entropy of aluminum vacancy hopping and low frequency vibrational modes. Under molecular dynamics a subset of Al atoms displays nearly liquid diffusive motion.

DOI: 10.1103/PhysRevB.75.014207 PACS number(s): 61.44.Br, 71.23.Ft, 61.66.Dk

## I. INTRODUCTION

Decagonal quasicrystals occur as metastable phases in the binary alloy Al-Co (Refs. 1–3) and as stable phases in the Al-Co-Ni ternary.[4] Knowledge of the complete phase diagrams of these alloy systems can aid the understanding of the structures and stability of the quasicrystals. Unfortunately, but not surprisingly, these phase diagrams remain poorly understood precisely at the compositions of greatest importance, with a proliferation of competing and imperfectly characterized crystal structures. Some of these structures are quasicrystal approximants, which means that they are crystals containing local structures that can be extended quasiperiodically to match the global quasicrystal structure.

The regime $0.23 < x_{Co} < 0.26$ is the most controversial with the various experimentally observed phase diagrams differing in the total number of phases and the composition sequence in which they occur.[5–11] Even the most recent of these are of questionable validity because they violate the "rule of thumb" that phases close in composition should not coexist over an extended temperature range.[12] Our calculations suggest revisions in the assessment of low temperature stability, where experiments are unreliable due to diverging equilibration times.

The most recent experimental determinations agree on the identities and approximate structures of the phases, but not their sequence. According to Grushko,[10] starting from pure Al.cF4 (LT), they are $Al_9Co_2$.mP22 (LT); O-$Al_{13}Co_4$.oP102 (LT); *M*-$Al_{13}Co_4$.mC102 (LT); *Y*-$Al_{13}Co_4$.mC34-1.8 (HT); *Z*-$Al_3Co$ (LT); $Al_5Co_2$.hP28 (LT); AlCo.cP2 (LT); and Co.hP2 (LT). Goedecke and Ellner[7] interchange the relative composition of the *M*- and *Y*-$Al_{13}Co_4$ phases, suggesting that *M*-$Al_{13}Co_4$ is Co-richer than *Y*-$Al_{13}Co_4$. Neither *Y*- nor *Z*- have rigorous structure determinations. However, the structure types are agreed on, with *Y*- of structure similar to $Al_{13}Os_4$.mC34, though probably with about 1.8 Al vacancies per cell, similar to $Al_{75}Co_{22}Ni_3$. The structure of the *Z*-phase is known to be a quasicrystal approximant and is sometimes called $\tau^2$-$Al_{13}Co_4$.

We apply first-principles total energy calculations to compare cohesive energies of known and hypothetical structures (Fig. 1 and 2). Our calculational methods are discussed in Sec. II. The alloy phase diagram at low temperature consists of structures whose energies form the convex hull of cohesive energy as a function of composition. Although our focus is on the Al-Co binary system, we exploit knowledge of the Al-Co-Ni ternary in this study. The known complex quasicrystal approximant phases with composition close to $Al_{13}Co_4$ [Pearson symbols oP102 (Ref. 13) and mC102 (Refs. 14 and 15)], previously believed stable down to low temperatures, are actually either metastable or stable only at high temperature.

Our main goal is to explain the stability of $Al_{13}Co_4$, which must be due to some entropic effect. We examine possible sources of entropy including disorder in "puckering" pattern (Sec. III B), vacancy disorder (Sec. III A), and vibrational entropy (Sec. IV). Our results show that a combination of vacancy and vibrational entropy may be sufficient to stabilize $Al_{13}Co_4$ at high temperatures. We then perform a high temperature molecular dynamics simulation (Sec. V) that suggests the vacancies and vibrations combine to create a nearly liquid diffusive behavior among a subset of Al atoms.

Another reported structure, $Al_3Co$.oI96, which had previously been presumed metastable, turns out to be preferred and may be the true low temperature state. Although structurally related to the mC102/oP102 phases, oI96 is not itself a "good approximant." While oP102 and mC102 alternate flat and puckered atomic layers to achieve a periodicity of 8 Å along the pseudo fivefold axes, oI96 alternates flat layers with pairs of puckered layers for a net 12 Å periodicity. It is closely related to a known high temperature phase, $Al_{13}Co_4$.mC32, which has only a 4 Å periodicity, consisting only of flat layers.

## II. METHODS

We calculate total energies within electronic density functional theory using the plane-wave program VASP.[16,17] Our calculations, which employ PAW potentials[18] in the PW91 generalized gradient approximation,[19] are carried out at a fixed cutoff energy of 268 eV. We relax atomic positions and lattice parameters, and select *k*-point meshes to achieve a

 

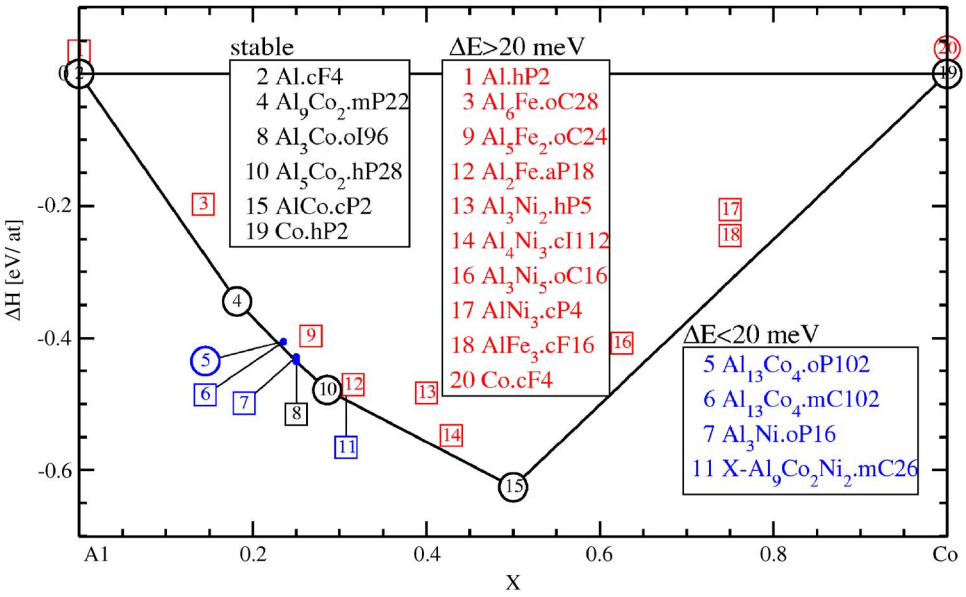


FIG. 1. (Color online) Enthalpies of formation in the Al-Co binary alloy system over its full composition range. Notation: heavy circles=known (or claimed) low temperature phases, light circles=known high temperature phases, diamonds =known metastable phases, and squares=unreported (hypothetical) structures. Structures are labeled by their compound names followed by their Pearson symbols.

target precision of 0.001 eV/atom on all relative energies. More details of similar calculations can be found in Ref. 20.

Structures for study are selected from established experimental phase diagrams,[5] collections of intermetallic structures,[21] and recent original literature. We name our structures according to the Pearson convention which lists point symmetry, translational symmetry, and the number of atomic positions per cell. For example, mC102 is monoclinic, C-centered, with 102 atomic positions (possibly fractionally occupied) per cell. Our study of the Al-Co binary system includes for comparison purposes structures present in the Al-Fe and Al-Ni binaries (with Co substituting for Fe and Ni), and also the Al-Co-Ni ternary considered as a pseudobinary (substituting Co for Ni).

Spin polarization was considered but found to be present only at compositions $x_{Co}>0.5$. The VWN spin-interpolation[22] is used for the *XC* potential.

Given cohesive energies for all structures, we calculate enthalpies of formation by subtracting each cohesive energy from the tie-line joining each pure element in its lowest energy configuration. The structure (or coexistence of two structures) that minimizes the enthalpy is the thermodynamically stable structure for a given composition at low temperature. These form a "convex hull" of enthalpy versus composition, which we identify using the program qhull.

Our chief result is illustrated in Fig. 1 and 2. Evidently, we have a nearly perfect agreement with the experimentally determined phase diagram. With the exception of the $Al_{13}Co_4$ structures, all known low temperature phases lie on the convex hull. Likewise, the hypothetical structures drawn from chemically similar Al-Fe and Al-Ni systems lie above the convex hull. The faithfulness with which the experimental phase diagram is reproduced, and the ability to distinguish among chemically similar compounds is outstanding. All our data from these (and other) calculations is available on the WWW.[23]

The sole area of discrepancy between our results and the experimentally reported phase diagram is in the range $0.23<x_{Co}<0.26$, precisely the area in which the experimental phase diagram is unsatisfactory in any case. Our calculated results can thus shed light on the experimentally unresolved questions. In particular, since we have no kinetic limitations on our ability to reach the energetically optimal structure, we may be able to distinguish true low temperature phases from high temperature or metastable phases.

The main conclusion we draw is that the oP102/mC102 phases, believed stable at low temperatures, must be either metastable or high temperature (HT) phases, because they lie significantly above the convex hull. From our study of intrinsic configurational disorder and thermal vibrations, in these structures we find a large entropy sufficient to stabilize the oP102/mC102 above temperatures of about $T=750$ K. Thus we propose they are actually HT phases.

The $Al_3Co$.oI96 structure lies essentially on the tie-line from $Al_9Co_2$ to $Al_5Co_2$. It may be the true low temperature phase, or may be marginally unstable. Calculations employing the GGA[19] place it 2.6 meV/atom below the tie-line, implying stability, while calculations (not shown) employing the PBE place it 1.7 meV/atom above, indicating the range of uncertainty in calculated enthalpy differences. This discrepancy only affects oI96, the $Al_{13}Co_4$ family remains unstable by about 5 meV/atom under all choices of *XC* potential (see Fig. 2).

### III. $Al_{13}Co_4$ FAMILY

The two structures $Al_{13}Co_4$.oP102 and $Al_{13}Co_4$.mC102 share identical local building blocks and differ only in their global arrangement. To understand these structures it is helpful to use the elementary cluster known as a pentagonal bipyramid[24,25] (PB) illustrated in Fig. 3. The PB is a three-dimensional 23-atom cluster comprising a "flat" equatorial layer consisting of alternating Al and Co pentagonal rings centered by a single Al atom, and two "puckered" cap layers consisting of a small Al pentagon centered by a Co atom. The puckered layer Co atoms are displaced slightly away from their surrounding Al pentagons due to their repulsion from the PB center Al atom. The PB cluster alternates with

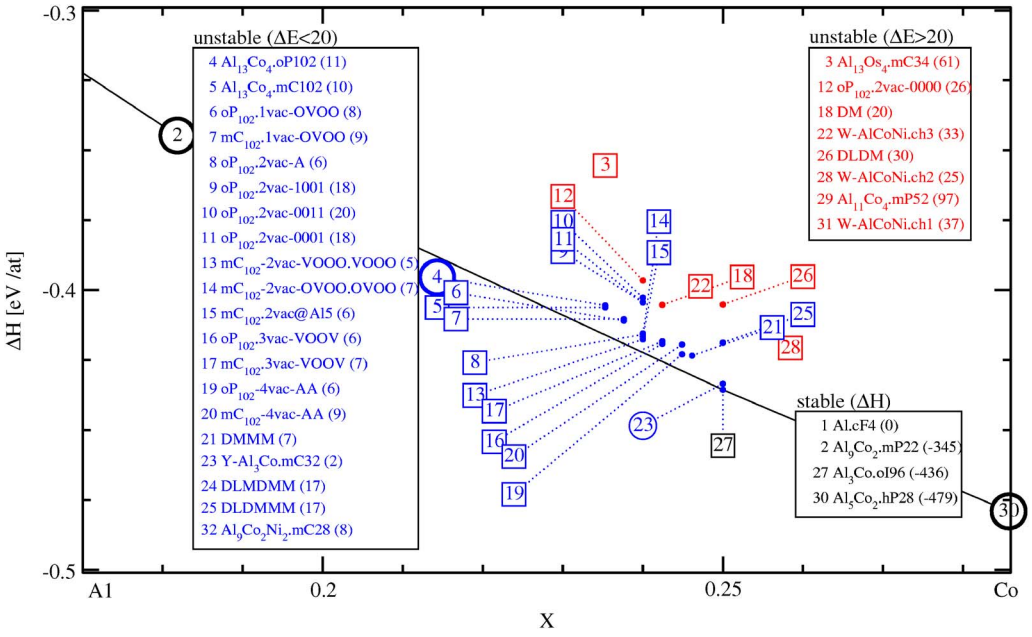


FIG. 2. (Color online) Enthalpies of formation of $Al_{1-x}Co_x$ over the range $0.17 \leq x \leq 0.29$. Notation as in Fig. 1.

junction layers to form an infinite column (the "PB column") with a fivefold symmetry broken only by the distribution of Al atoms inside the junction layers.

The stacking sequence of layers is thus the PB bottom tip (with a negative Co displacement marked "–"), next comes the PB center flat layer, then the PB top tip (with a positive Co displacement marked "+"), and finally a flat layer junction. The mean layer spacing is 2 Å, and the four layers indicate an 8 Å vertical periodicity. In the oP102/mC102 structures, layers are globally flat or puckered meaning that each flat layer consists entirely of PB centers and junctions, while each puckered layer consists entirely of PB±tips. Consider a "tube" of radius=PB radius centered on the PB central axis. Inside this tube the sequence of atoms is PB tip (Co– at center), PB center (1 Al at center), PB tip (Co+ at center), PB junction.

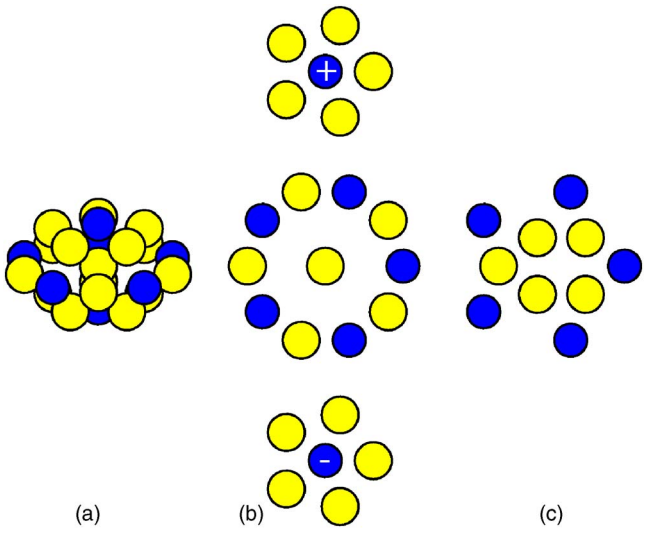


FIG. 3. (Color online) PB cluster. (a) Three-dimensional view of PB cluster. (b) Exploded view showing Al-centered flat layer together with top and bottom caps marked, respectively, + and –. (c) PB junction layer. Color coding: yellow=Al and blue=Co.

All the Co atoms, and most of the Al atoms, are contained in PB clusters. This can be seen by examining Fig. 4. The remaining Al atoms are mainly located in flat "junction" layers, which join PB clusters stacked along the vertical direction. Each junction contains up to 5 Al atoms. In Fig. 4 some of these junction Al sites are labeled with numbers. Some flat layer Al atoms (e.g., numbers 5 and 14) are shared between neighboring clusters. Finally, there are four "glue" Al atoms in the puckered layers (labeled number 18) that do not belong to any clusters or junctions.

Viewing a single puckered layer, a tiling can be defined by joining Co atoms at PB tips. This particular structure contains only one type of tile, an elongated hexagon with edge length 6.5 Å. At the same time, the flat layer exhibits a tiling by pentagons and rhombi, with edge length 4.8 Å, formed by joining Co atoms.

It turns out that $Al_{13}Co_4$.mC102 and $Al_{13}Co_4$.oP102 define two different planar tilings of hexagon tiles (Fig. 5). Meanwhile, the pattern of Co displacements (equivalently the pattern of flat layers in which the PB is centered) assigns an "Ising" ± spin to each vertex.[25] Finally, there can be vacancies which tend to concentrate among the Al atoms of PB junctions, as seen in Fig. 4. There are thus three important types of configurational freedom and associated disorder to consider: vacancies, layer puckering, and tiling. We consider each of these in the following three sections.

Also of interest is $Al_{11}Co_4$.mP52, a QC approximant with a 4 Å periodicity.[26] This curious structure alternates motifs similar to the flat and puckered layers of mC102 and oP102, but with only a 4 Å periodicity so that the "flat" layers cannot be perfect mirrors, and hence are not perfectly flat. We find it is quite high in energy, and also that both layer types relax to a perfectly flat structure. It is structurally related to

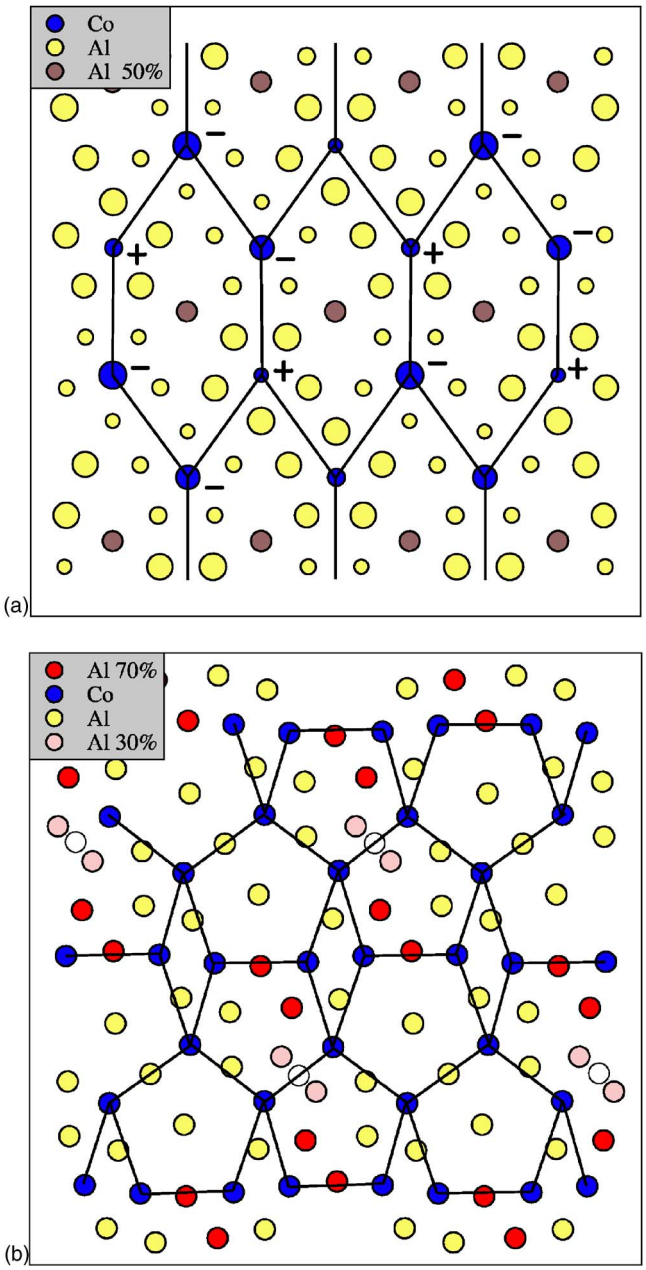


FIG. 4. (Color online) Puckered (top) and flat (bottom) layer structures of $Al_{13}Co_4$.mC102. Blue atoms are Co, yellow are Al, while red, brown, and pink indicate fractional occupancy of 0.7, 0.5, and 0.3, respectively, according to the structure determination of Hudd (Ref. 14). Numbers are orbit labels. Large/small atoms indicate displacement down/up.

the ternary $X$-$Al_9Co_2Ni_2$.mC26 phase,[27] which is more Co-rich.

### A. Vacancy disorder

The structure determinations[14,15] of $Al_{13}Co_4$.mC102 reported partially occupied Al sites, especially among PB junction sites in the flat layers. The partially occupied sites are shaded and labeled in Fig. 4. Vacancies are not reported in recent evaluation oP102,[13] but abnormally large thermal factors in those structures may indicate partial occupancy. Vacancies are plausible because these sites are overcrowded, with Al-Al spacing as low as 2.3 Å, where 2.9 would be more favorable. In this section we explore the role of vacancies from both an electronic structure and statistical mechanical point of view. We show that a small number of vacancies lowers the enthalpy, but not sufficiently to yield low temperature stability. However, when vacancy entropy is included the structure could achieve high temperature stability.

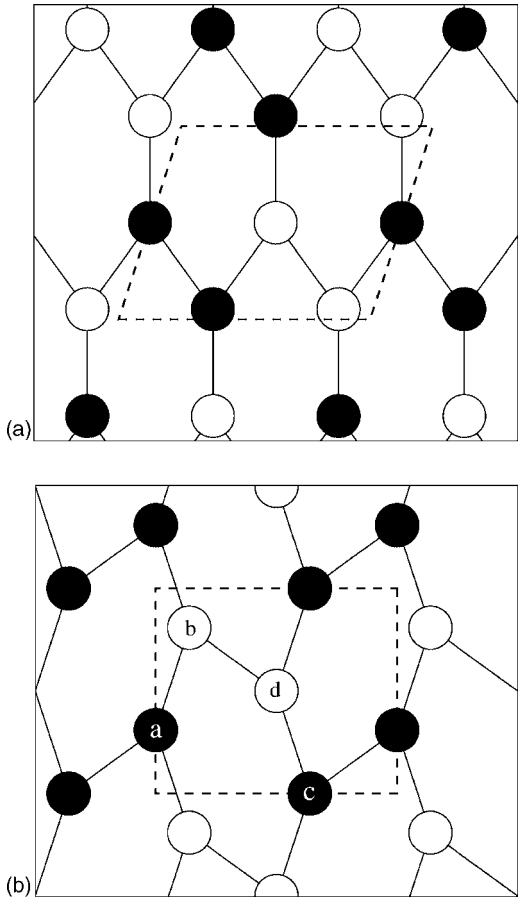


FIG. 5. Tilings and puckering patterns of mC102 and oP102. Black/white circles denote up/down puckering. Labels in oP102 indicate the set of independent vertices for studies of puckering energies.

First we examine the vacancy energetics. Inspecting Fig. 2 reveals that a few vacancies can lower the enthalpy, with $\Delta E$ dropping from +12 meV/atom to +6 meV/atom. Limited vacancy formation can be understood from the perspective of electronic structure by inspecting the electronic density of states illustrated in Fig. 6. Notice that the density of states contains a strong pseudogap near the Fermi energy. For fully occupied $Al_{13}Co_4$.mC102 the Fermi energy lies just to the right-hand side of the gap. Introducing Al vacancies moves $E_F$ towards the bottom of the pseudogap, which can lower the band structure energy.

The pseudogap has a steep left side and a relatively shallow right side. This can explain the trend in stability of mC102 For Al-$TM$ alloys with $TM$ a first-row transition metal. Recall the sequence of chemical valence runs…, Mn,

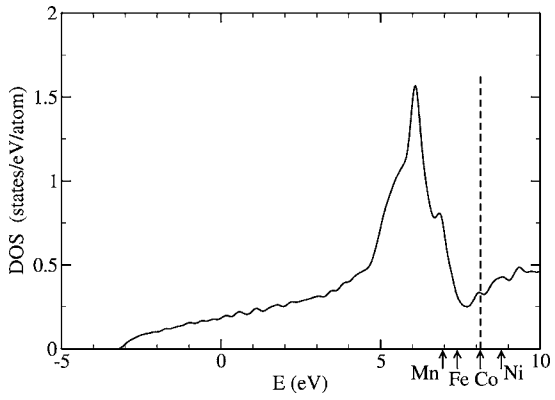


FIG. 6. DOS of fully occupied $Al_{13}Co_4$.mC102. Arrows indicate $E_F$ for $Al_{13}TM_4$ with (lowest to highest) $TM$=Mn, Fe, Co, and Ni calculated within the rigid band model.

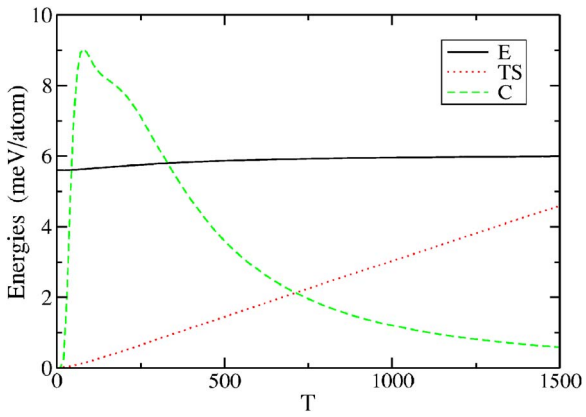


FIG. 7. (Color online) Vacancy heat capacity, internal energy, and entropy.

Fe, Co, Ni,…. The Fermi energies in Fig. 6 were calculated within the rigid band model. In a 102 atom unit cell of $Al_{13}Co_4$, with stoichiometry $Al_{78}Co_{24}$, replacing Co with Mn, Fe, or Ni changes the total number of electrons by −48, −24, or +24, respectively. We calculated the DOS for fully occupied $Al_{13}Co_4$.mC102, then integrated the DOS from EF(Co) up or down to the energy that would match the change in electron count.

When $TM$=Mn, the structure is electron-poor and $E_F$ lies well below the gap. mC102 is energetically unfavorable. When $TM$=Fe, $E_F$ lies at a nearly optimal point just at the left-hand edge of the gap. Indeed, our calculations[23] reveal that mC102 is stable at low temperature in $Al_{13}Fe_4$, and vacancies are unfavorable. Likewise, we confirm stability of fully occupied $Al_{13}Ru_4$ (Ru lies below Fe in the periodic table) and confirm metastability of $Al_{13}Rh_4$ (Rh lies below Co). When $TM$=Co, the structure becomes slightly electron-rich. Low temperature stability is lost and vacancies are favored. Finally, when $TM$=Ni $E_F$ moves above the pseudogap and mC102 is energetically unfavorable.

The distribution of vacancies among aluminum atoms in mC102 (see shading in Fig. 4) and oP102 provides a source of configurational entropy. We analyze this in detail for mC102, but similar results are found for oP102. The string of six shaded Al atoms that lie in the flat layer, where two PB junctions occur side-by side, is overly dense in Al. In this string we find Al spacings as low as 2.31 Å. For comparison the peak of the AlAl pair correlation function in mC102 occurs at 2.83 Å. The entire string of six is reported to be partially occupied in the structure solution of Hudd.[14] Only the inner four possess vacancies according to the structure solution of Freiburg.[15]

We investigated the stability and energetics of structures with Al vacancies inserted at these sites (see Fig. 2) and found that removal of one or two Al atoms out of the string of six is favorable. It turns out that introduction of vacancies at the end points of the string of six, at sites of type[15] Al3, leads to large displacements of the neighboring Al6 atoms to fill the vacancy. The Al3 vacancies are thus unstable, consistent with Freiburg's observation of full occupancy. A puckered layer site, Al15 is partially occupied according to Hudd but not Freiburg. We found the vacancy at this site to be mechanically stable, but energetically costly (1.5 eV per vacancy).

The other vacancies, at sites Al6 and Al7, are energetically favorable, reducing $\Delta E$ from +10.1 meV/atom to, respectively, +5.9 and +6.7 meV/atom. Vacancies at Al6 sites are mechanically stable, with only small relaxations of adjacent atoms. In contrast, when an Al7 site is vacant the adjoining Al7 atom displaces towards the midpoint of the bond that joins them. The resulting positions lie slightly off the midpoint at the locations indicated with open circles in Fig. 4.

To gauge the thermodynamic impact of Al vacancies, we evaluate the partition function

$$Z = \sum_{config} \exp -(\Delta E)/k_B T. \quad (1)$$

We restrict our sum to the set of configurations containing just one vacancy per 51-site primitive cell and include only the vacancies at Al6 and Al7 sites. From the partition function we obtain the free energy, enthalpy, entropy, and heat capacity by the usual methods of statistical mechanics. $G=-k_BT \log Z$, $S=-\partial G/\partial T$, $H=G+TS$, $C_p=T\partial S/\partial T$.

If the reduction in free energy due to vacancy entropy at high temperature exceeds the unfavorable enthalpy of mC102 compared with $Al_9Co_2$.mP22 and $Al_5Co_2$.hP28, then vacancy disorder can lead to high temperature thermodynamic stability of mC102. Implicitly we assume vacancy entropy can be neglected in mP22 and hP28 (our calculations find the lowest vacancy formation energy is 560 meV). We also assume the vacancy entropy of mC102 is large compared to any differences in vibrational entropy among these structures. Because the terms in Eq. (1) are weighted according to $\Delta E$, the enthalpy difference between our vacancy structures and the tie-line connecting mP22 to hP28, thermodynamic stability occurs if $G<0$.

As temperature rise up to the peritectic melting temperature $T_m$=1366 K, we see that $TS$ approaches $E$ but does not reach it (see Fig. 7). To stabilize $Al_{13}Co_4$, an additional effect is needed, which turns out to be the vibrational entropy of low frequency phonons (see Sec. IV).

TABLE I. Puckering pattern energies of oP102 relative to experimentally observed pattern (meV/atom).

| Pattern | $+J1$ | $-J1$ | $+J2$ | $-J2$ | $\Delta E$ | Fit |
|---|---|---|---|---|---|---|
| 0000 | 6 | 0 | 4 | 0 | 20.3 | 22.1 |
| 0001 | 3 | 3 | 2 | 2 | 12.1 | 11.6 |
| 0011 | 4 | 2 | 0 | 4 | 13.7 | 8.9 |
| 0101 | 2 | 4 | 0 | 4 | 0 | 5.0 |
| 1001 | 0 | 6 | 4 | 0 | 12.0 | 10.5 |

Regardless of the high temperature stabilization mechanism, our study of vacancy energetics shows that neither $Al_{13}Co_4$.mC102 nor $Al_{13}Co_4$.oP102 is stable at low temperature at any composition. Our results also indicate that 2–4 Al vacancies per 102 atom cell are favorable in both $Al_{13}Co_4$.mC102 and $Al_{13}Co_4$.oP102, placing their phase fields slightly to the right of $x=0.2353$. Vacancies are favored owing to the crowding of Al atoms in flat layers and to the location of the Fermi energy slightly above a pseudogap.

### B. Puckering disorder

We can define Ising model couplings between neighboring tiling vertices by exhaustively forming all spin patterns on the vertices of a single unit cell and comparing their energies. To eliminate coupling between the puckering pattern and the distribution of vacancies among junction layer Al atoms, we adopt a simple rule that places a single Al atom midway between sites of types 4 and 13 (see Fig. 4). In this way, a single Al atom lies in each flat layer along each hexagon tile edge. This rule can be applied to either mC102 or oP102, but we choose to focus on oP102. The unit cell contains 100 atoms and two vacancies.

Our results, which are summarized in Table I, can be fit roughly using only two coupling constants $J_1$ and $J_2$ and an overall constant $J_0$. The coupling $J_1$ applies to near-neighbor PB columns that share a pentagon edge (i.e., 6.5 Å hexagon tiling vertices connected by a tile edge). $J_2$ applies to next-nearest-neighbor PB columns that are joined only at a pentagon vertex (i.e., tiling vertices adjoining a 72° vertex of the 6.5 Å hexagon tiling. A given puckering pattern is specified by the Ising spin variables on each distinct PB column *abcd* [see Fig. 5(b)].

We fit $\Delta E \approx J_0 + J_1 N_1 + J_2 N_2$ with $J_0=11.6$, $J_1=1.0$, and $J_2=1.2$. Since both $J_1$ and $J_2$ are antiferromagnetic, the ordering is partially frustrated. Still, a unique ground state pattern exists and matches the experimentally observed pattern, for both oP102 and mC102. The couplings are antiferromagnetic owing to the interactions of junction layer Al atoms. Examine the flat layer structure (Fig. 4) and note the Al atom lying on the shared pentagon edge joining near-neighbor PB columns. This atom displaces towards the interior of the junction layer pentagon. If two junction layers were at the same level, this displacement would be frustrated. Now examine the thin rhombus and the two PB columns that touch at each acute vertex of this rhombus. The Al atom inside this acute angle is repelled by the PB junction layer Al atoms. If two junction layers were at the same level, this displacement would be frustrated.

The energy units used above are meV/atom in an 8 Å periodic 100 atom cell. We can multiply each value by 50 to obtain the coupling strength per flat layer, $J_1=50$ and $J_2=60$ meV, which is of order $k_BT$ at $T=700$ K, suggesting the possibility of thermal disorder in the puckering pattern. But to investigate the possibility of puckering disorder contributing to the entropy, we need to generalize our Ising model to three dimensions. This is because the entropy of in-plane disorder grows like the 2/3 power of volume and hence is subextensive. Thus we consider stacking disorder in the puckering sequence along a column of PBs.

Reversal of the puckering sequence is created by placing 2 Al atoms inside two consecutive flat layers, averaging the structure of a 1 Al PB center and a 3 Al junction layer. Interestingly, this type of "averaged" PB decoration is observed in the *W*-phase of Al-Co-Ni.[28,29] We created a realization of this structure by taking a quarter cell of mC102 (4 Å periodicity and 1/2 of the long axis) and replacing the PB center Al with an Al pair to yield an mC26 structure, which turns out to be a variant of the *X*-$Al_9Co_2Ni_2$ phase[27] with some chemical species swaps. The resulting energy exceeds our best mC102 structure by 35 meV/atom and contains two reversals per cell. The energy cost for this reversal is $35\times 26/2=455$ meV which we take as the strength of vertical coupling $Jz$ in our Ising model. The vertical coupling is so strong we conclude that disorder in the puckering pattern is of no thermodynamic significance for either mC102 or oP102. However, the in-plane $J1$ and $J2$ couplings are relevant for determining the globally ordered puckering pattern.

### C. Tiling disorder

Note in Fig. 2 how close mC102 and oP102 are in energy. This near degeneracy persists across a broad range of composition and suggests that perhaps any tiling of the plane by hexagons would be nearly as good. Indeed, in addition to the elongated hexagons present in the mC102 and oP102 tilings, there are a boat shape and a star shape, which have been observed in Al-Co-Ni quasicrystal approximants such as the *W*-phase. This set of shapes belong to an ensemble of tilings known as two-level, or HBS, tilings. We expect this tiling ensemble to be highly degenerate, but uniformly unfavorable, in energy. Thus it may characterize the metastable binary Al-Co quasicrystal state.

One specific HBS tiling has a partially known structure, known as "Z" and also as $\tau^2$-$Al_{13}Co_4$. While its stacking periodicity is still 8 Å, its lattice parameters in the plane of the tiling are $\tau^2$ times larger than mC102. One possible realization of such a structure[30] is reproduced in Fig. 8. Curiously, this $\tau^2Al_{13}Co_4$ structure can be considered as a *supertiling* of the ordinary mC102 structure, in which *H*, *B*, and *S* tiles of a 6.47 Å edge length combine to form a larger hexagonal tile of edge length $\tau^2\times 6.47=16.94$ Å. This structure can be decorated with PB columns and other motifs as discussed in Refs. 25 and 29 and should contain approximately 350 atoms. It should be feasible to refine the tiling structure, puckering pattern, and site occupancies using methods similar to those employed above.

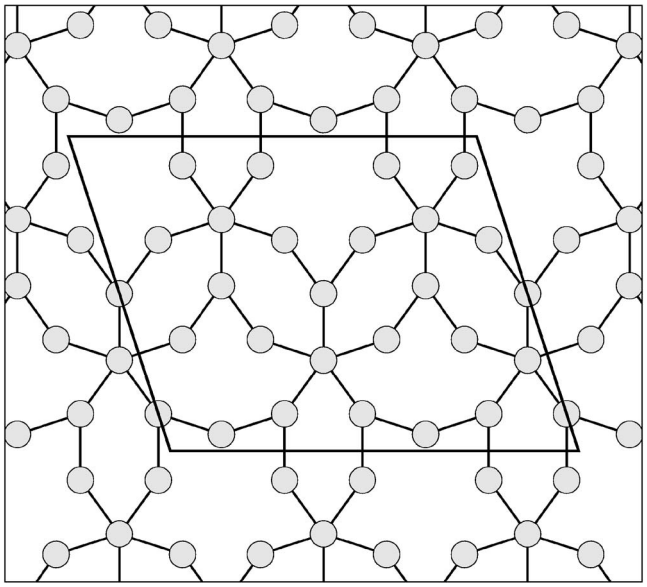

FIG. 8. Possible tiling for $\tau^2$-$Al_{13}Co_4$ phase.

## IV. VIBRATIONAL PROPERTIES

We calculated the vibrational density of states and vibrational free energy of the main Al-Co compounds. Including the vibrational free energy allow us to extend our knowledge of stability from the limit of vanishing temperature, where only the enthalpy is relevant, to finite temperature. It turns out that $Al_{13}Co_4$ exhibits a small excess of low frequency modes associated with the disordered flat layer aluminum atoms. These contribute sufficient vibrational entropy that, combined with the previously identified configurational entropy of vacancies, is sufficient to stabilize the quasicrystal approximant structure at elevated temperature.

To calculate the vibrational density of states, a complete set of independent atomic displacements was performed within single primitive cells of each structure. For $Al_{13}Co_4$ we chose a 51-site primitive cell of mC102, with a single Al vacancy at position No. 13. The vibrational spectrum was calculated using the "fitfc" method of the ATAT toolkit.[31] This method calculates the second derivatives of total energy $E$

$$\frac{\partial^2 E}{\partial \mathbf{R}_i \partial \mathbf{R}_j} \tag{2}$$

for atom positions $\mathbf{R}_{i,j}$ within an interaction range which we took as 4 Å. The vibrational density of states (DOS) was then calculated using a full Brillouin zone integration, so that the structural details in the resulting DOS are true intrinsic properties of the model.

Figure 9 illustrates the results. Of particular interest is the comparison between $Al_{13}Co_4$ and the competing crystal structures $Al_9Co_2$ and $Al_5Co_2$. Note the slight excess density of states at low frequency in $Al_{13}Co_4$. Such an excess is observed experimentally.[32] We attribute these modes to flat-layer Al atoms because they disappear when the flat layer sites are fully occupied.

We checked that our results are not significantly influenced by the choice of interaction range, or by the choice of

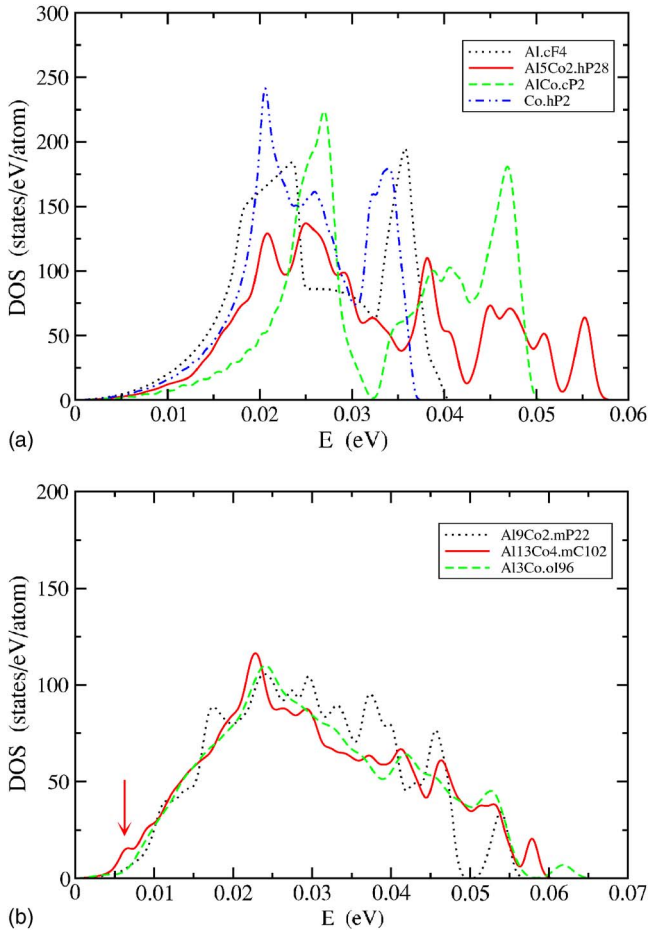


FIG. 9. (Color online) Vibrational densities of states for Al-Co compounds. We separate those of composition $0.1818 < x_{Co} < 0.25$ from the remainder, for clarity. Arrow indicates excess low frequency modes.

electronic or phonon $k$-point densities. Also, our density of states is closely matched with an alternate method based on velocity autocorrelation functions obtained from molecular dynamics.

Vibrational free energies are calculated as

$$f_{vib}(T) = k_B T \int DOS(\omega) \log 2 \sinh \hbar\omega / 2k_B T d\omega. \tag{3}$$

Low frequency modes that can be excited at low temperatures contribute strongly to the vibrational entropy, reducing the free energy. The difference between the vibrational free energy of $Al_{13}Co_4$ and a composition-weighted average of the free energies of $Al_9Co_2$ and $Al_5Co_2$ is plotted in Fig. 10. Evidently, the low frequency modes of $Al_{13}Co_4$ lend it thermodynamic stability as temperature rises. The free energy reduction due to vibrations reaches 7 meV/atom at the melting temperature $T_m = 1366$ K. Combining vacancy and vibrational entropy, the free energy of $Al_{13}Co_4$ falls below the tie-line of coexisting phases at nearby compositions when temperature exceeds $T = 750$ K.

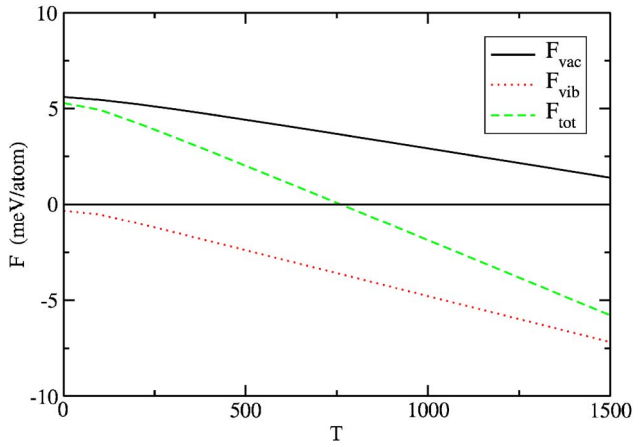


FIG. 10. (Color online) Vacancy, vibrational, and total free energy.

## V. MOLECULAR DYNAMICS

Given the presence of vacancies and associated low frequency phonons, we performed a molecular dynamics simulation for a single 102-site unit cell of $Al_{13}Co_4$.mC102. We introduced vacancies at the initial positions of site class No. 13, and evolved the system at $T=1350$ K for 8.5 ps. Forces were calculated from first-principles using VASP. Figure 11 illustrates the result by projecting the trajectories of all atoms in the two layers illustrated in Fig. 4 into a plane. Clearly Al atoms diffuse easily along the channels defined by the strings of four Al atoms where the vacancies occur.

Rather than decompose the entropy into separate vacancy and vibrational contributions (a decomposition that is clearly defined only in the limit of low temperature), we could estimate the combined entropy directly by treating the string of Al atoms as a liquid. Treat Al atoms as hard spheres of diameter $a=3$ Å. A string of four Al atoms defines a channel of length 12 Å, which will be occupied by three spheres. The translational partition function may be evaluated as

$$Z_{liquid}=\frac{1}{\Lambda^3}\int_0^a dx_1\int_{x_1+a}^{2a} dx_2\int_{x_2+a}^{3a} dx_3=\frac{9}{2}\left(\frac{a}{\Lambda}\right)^3. \quad (4)$$

The thermal de Broglie wavelength

$$\Lambda=\sqrt{\frac{2\pi mk_BT}{h^2}}=0.09\ \text{Å} \quad (5)$$

at $T=1350$ K. In contrast, if the atoms remained bound within a distance $b$ of their nominal lattice positions, we can estimate the partition function of each Al atom as

$$Z_{solid}=\frac{1}{\Lambda^3}\left(\int_{-b}^{b} dx\right)^3=(b/\Lambda)^3. \quad (6)$$

From Fig. 11 it appears that $b\approx 0.5$ Å. From the partition functions we calculate the free energy as $F=-k_BT\log Z$. Putting in numbers for $T=1350$ K, and dividing by 50 (the number of atoms in the primitive cell containing a single Al string) we find $F_{liquid}=0.024$ eV/atom, and $F_{solid}=0.010$ eV/atom. So the liquid entropy lowers the free energy below the solid by about 10 meV/atom, consistent with our prior estimates.

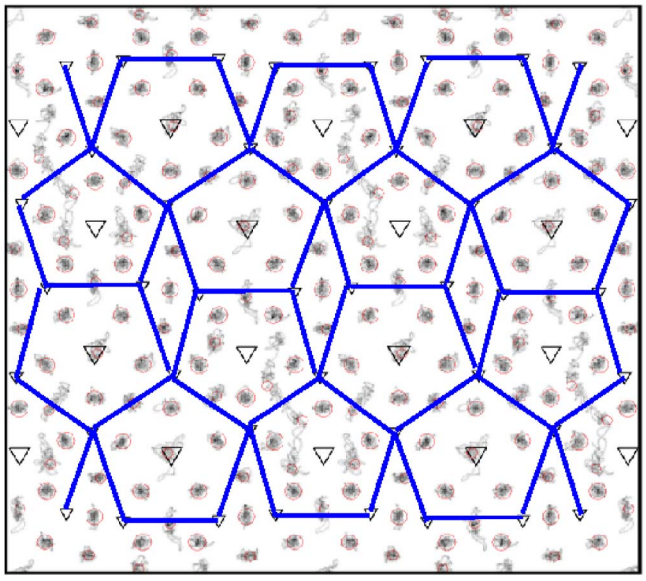

FIG. 11. (Color online) Projected molecular dynamics trajectories. Flat layer tiling indicated in blue, Al and *TM* atom positions indicated via red circles and black triangles, respectively.

## VI. $Al_3Co$ VARIANTS

Several structures, $Al_{13}Co_4$.mC32, $Al_{13}Os_4$.mC34, and $Al_3Co$.oI96 are closely related and seem plausible for compositions around $Al_3Co$. They all may be viewed as different stackings of the same average layer with slight modifications. The layer modifications are denoted *D* for dense, *M* for medium, and *L* for loose. *D* has 13 Al, *M* has 12 Al, and *L* has 10 Al. The mC34 structure is *DD*, mC32 is *MM*, and oI96 is *DLDDLD*. Relative horizontal translations of the layers lead to either monoclinic or orthorhombic structures. Inspecting the patterns of large Co (outlined) reveals partial PBs. Roughly speaking the PB equators correspond to *L* layers, fully occupied PB junctions correspond to *D* layers. The *M* layer corresponds to a PB junction with the sites of type (Hudd notation) Al4 and Al13 replaced by their average position as illustrated in Fig. 4.

The structure we label as $Al_{13}Co_4$.mC32 has not actually been reported in the literature in the Al-Co binary system. Rather, it appears in the Al-Co-Ni ternary as the "*X*" phase (Steurer and Zhang) and is given structure $Al_{13}(Co,Ni)_4$.mC34-1.8. The notation mC34-1.8 indicates the introduction of 1.8 vacancies into the $Al_{13}Os_4$.mC34 structure. The *X* phase extends almost to the Al-Co binary, with Ni content as low as 3% Ni. The structure we label Al3Co.oI96 also comes from the ternary, reported[33] as the "$Y_2$" phase of $Al_9Co_2Ni$.oI96.

Our results, as listed in Table II show that the fully occupied $Al_{13}Os_4$.mC34 structure is highly unfavorable, suggesting that atoms are too crowded in the dense *D* layers. Relieving the overcrowding by replacing *D* with *M* leads to the far more stable structure we refer to as $Al_{13}Co_4$.mC32. Be-

TABLE II. Energies of mC32-mC34-oI96 family. Atomic volume units are Å$^3$/atom. Energy units are meV/atom.

| Sequence | Structure | V/atom | $\Delta H$ | $\Delta E$ |
|---|---|---|---|---|
| *DD* | $Al_{13}Os_4$.mC34 | 14.20 | −360.1 | 60.4 |
| *DLDM* | Hypothetical | 14.49 | −409.7 | 30.1 |
| *DM* | Hypothetical | 14.33 | −409.9 | 20.0 |
| *DLDMMM* | Hypothetical | 14.51 | −423.3 | 16.6 |
| *DLMDMM* | Hypothetical | 14.55 | −423.4 | 16.5 |
| *DMDM* | Hypothetical | 14.22 | −415.7 | 14.2 |
| *DMMM* | Hypothetical | 14.36 | −428.0 | 6.8 |
| *MM* | $Al_{13}Co_4$.mC32 | 14.52 | −438.0 | 1.8 |
| *DLDDLD* | $Al_9Co_2Ni$.oI96 | 14.44 | −439.9 | 0.0 |

cause each of these structures has a 4 Å repeat, each atomic layer is foced to be a mirror plane, and hence flat.

The most favorable of all, $Al_3Co$.oI96 (see Fig. 12), mixes *D* and *L* layers, with a stacking sequence of 12 Å periodicity. In this sequence, the *D* layers are puckered and the *L* layers flat. Apparently puckering of the *D* layer reduces overcrowding resulting in a favorable energy.

According to the data presented in Fig. 2, the enthalpy of oI96 is so low that it reaches the convex hull indicating low temperature thermodynamic stability. However, it just barely touches the hull, lying 1.8 meV/atom below the tie-line joining mP22 to hP28. Hence its stability is barely resolved within the expected accuracy of our methods. Indeed, using a different exchange correlation function, the PBE[34] instead of the PW91,[19] results in an energy 2.0 meV/atom *above* this tie-line. We therefore refrain from predicting that oI96 is actually a low temperature phase. Rather we suggest that further experiments are needed to determine if either mC32 or oI96 is stable, and over what temperature range.

Also in the ternary, but close to the binary Al-Co axis, there is a quasicrystal approximant W-AlCoNi.mC578, with lattice parameters $39.67\times8.15\times23.39$ Å at composition $Al_{72}(Co,Ni)_{28}$. The pseudo tenfold axis is parallel to *b* (lattice parameter 8.15 Å). This occurs close to the composition of the "basic Co-rich" decagonal phase, which also features an 8 Å stacking periodicity, and is presumably close in structure. The *W* phase structure contains mixed Al/*TM* occupancy sites. We assigned all *TM*=Co, and resolved the mixed occupancy in various ways, the most Al-rich of which we include in Fig. 2. Evidently this structure is rather far from low temperature stability as a binary. Indeed, even in the ternary we find it is not LT stable.

## VII. DISCUSSION

We calculated cohesive energies for many structures in the binary Al-Co alloy system. Our results generally support the main features of the experimentally assessed phase diagrams at low temperatures, but disagree in some details. The disagreements come entirely in a small composition range where recent experimental investigations have revealed and conflicting results. Of particular interest are the orthorhombic and monoclinic $Al_{13}Co_4$ structures, decagonal quasicrystal approximants, whose stability and vacancy concentrations are unclear experimentally. We find neither structure to be stable at low temperatures. Instead, the true low temperature state at this composition appears to be a phase-separated mixture consisting of $Al_9Co_2$ together with a structure of composition close to $Al_3Co$.

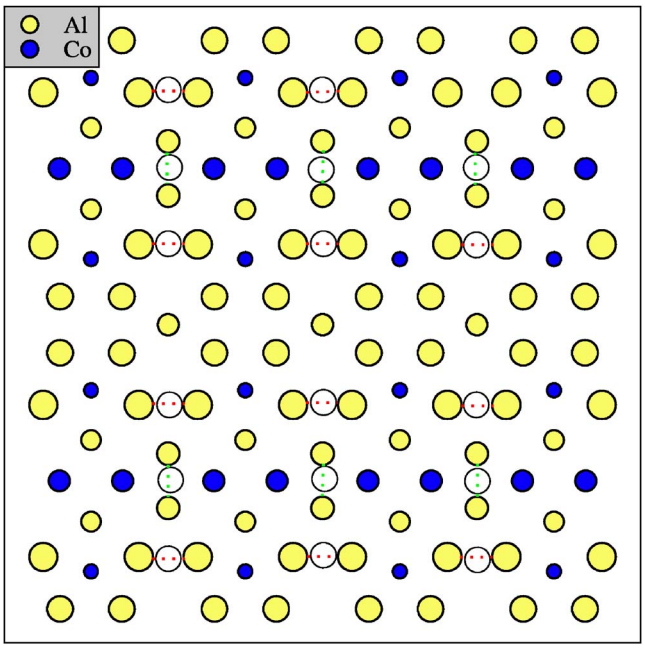


FIG. 12. (Color online) Dense "*D*" layer of $Al_3Co$.oI96. Convert to medium "*M*" by replacing Al pairs on vertical (green) bonds with single Al at center. Convert to loose "*L*" layer by replacing in addition horizontal (red) bonds. Fragments of an imperfect pentagon-rhombus tiling are outlined.

Small Al vacancy concentrations are energetically favorable, and the favored sites for vacancies are those flat layer Al sites reported as partially occupied by Hudd and Taylor.[14] The vacancy hopping entropy is nearly sufficient by itself to stabilize the structures close to their melting temperatures. We then combined the entropy of vacancy hopping together with an excess vibrational entropy due to low frequency vibrational modes associated with atoms located near the vacancies. The combination appears to be sufficient to stabilize $Al_{13}Co_4$ at temperatures above $T=750$ K.

Hopping energies and vibrational frequencies were calculated in the $T=0$ K limit, and were combined as distinct forms of structural disorder. An alternative picture we suggest, more appropriate to the realities of high temperature stability, is of liquidlike diffusion along one-dimensional channels. Such diffusion was explicitly observed through a solid state *ab initio* molecular dynamics simulation.

## ACKNOWLEDGMENT

This work was supported in part by NSF Grant No. NSF 0111198.

*Also at Institute of Physics, Slovak Academy of Sciences, 84228 Bratislava, Slovakia.
[1] C. Dong, G. B. Li, and K. H. Kuo, J. Phys. F: Met. Phys. **17**, L189 (1987).
[2] J. Menon, C. Suryanarayana, and G. Singh, J. Appl. Crystallogr. **22**, 96 (1989).
[3] X. L. Ma and K. H. Kuo, Metall. Trans. A **23**, 1121 (1992a).
[4] A.-P. Tsai, A. Inuoe, and T. Masumoto, Mater. Trans., JIM **30**, 463 (1989).
[5] *Binary Alloy Phase Diagrams*, edited by T. B. Massalski *et al.* (ASM International, Metals Park, OH, 1990).
[6] T. Goedecke, Z. Metallkd. **62**, 842 (1971).
[7] T. Goedecke and M. Ellner, Z. Metallkd. **87**, 854 (1996).
[8] T. Goedecke, Z. Metallkd. **88**, 904 (1997).
[9] B. Grushko, R. Wittenberg, K. Bickmann, and C. Freiburg, in *Proceedings of the 5th International Conference on Quasicrystals*, edited by C. Janot and R. Mosseri (World Scientific, Singapore, 1995), pp. 684–687.
[10] B. Grushko, R. Wittenberg, K. Bickman, C. Freiburg, J. Alloys Compd. **233**, 279 (1996).
[11] B. Grushko, C. Freiburg, K. Bickmann, and R. Wittenberg, Z. Metallkd. **88**, 379 (1997).
[12] H. Okamoto and T. B. Massalski, *Desk Handbook: Phase Diagrams for Binary Alloys* (ASM International, Metals Park, OH, 2000), Chap. Impossible and improbable alloy phase diagrams.
[13] J. Grin, U. Burkhardt, M. Ellner, and K. Peters, J. Alloys Compd. **206**, 243 (1994).
[14] R. C. Hudd and W. H. Taylor, Acta Crystallogr. **15**, 441 (1962).
[15] C. Freiburg, B. Grushko, R. Wittenberg, and W. Reichert, Mater. Sci. Forum **228-231**, 583 (1996).
[16] G. Kresse and J. Hafner, Phys. Rev. B **47**, R558 (1993).
[17] G. Kresse and J. Furthmuller, Phys. Rev. B **54**, 11169 (1996).
[18] G. Kresse and D. Joubert, Phys. Rev. B **59**, 1758 (1999).
[19] J. P. Perdew and Y. Wang, Phys. Rev. B **45**, 13244 (1992).
[20] M. Mihalkovič and M. Widom, Phys. Rev. B **70**, 144107 (2004).
[21] P. Villars, *Pearson's Handbook, Desk Edition* (ASM International, Materials Park, OH, 1997).
[22] L. W. S. H. Vosko and M. Nussair, Can. J. Phys. **58**, 1200 (1980).
[23] M. Mihalkovič and M. Widom, http://alloy.phys.cmu.edu
[24] C. L. Henley, J. Non-Cryst. Solids **153-154**, 172 (1993).
[25] E. Cockayne and M. Widom, Philos. Mag. A **77**, 593 (1998).
[26] X. Z. Li, N. C. Shi, Z. S. Ma, X. L. Ma, and K. H. Kuo, Philos. Mag. Lett. **72**, 79 (1995).
[27] S. Katrych, M. Mihalkovič, V. Gramlich, M. Widom, and W. Steurer, Philos. Mag. **86**, 451 (2006).
[28] K. Sugiyama, S. Nishimura, and K. Hiraga, J. Alloys Compd. **342**, 65 (2002).
[29] N. Gu, M. Mihalkovič, and C. Henley, Philos. Mag. **86**, 593 (2006).
[30] X. Z. Li and K. Hiraga, J. Alloys Compd. **269**, L13 (1998).
[31] A. van de Walle, M. Asta, and G. Cedar, J. Chem. Soc., Chem. Commun. **26**, 539 (2002); http://www.its.caltech.edu/~avdw/atat/
[32] M. Mihalkovič, H. Elhor, and J.-B. Suck, Mater. Sci. Eng., A **294-6**, 654 (2000).
[33] Y. Grin, K. Peters, U. Burkhardt, K. Gotzmann, and M. Ellner, Z. Kristallogr. **213**, 364 (1998).
[34] J. P. Perdew, K. Burke, and M. Ernzerhof, Phys. Rev. Lett. **77**, 3865 (1996).